Journal of Molecular Structure: THEOCHEM 901 (2009) 232–242

Contents lists available at ScienceDirect

Journal of Molecular Structure: THEOCHEM

journal homepage: www.elsevier.com/locate/theochem

Theoretical study of Au(I)–Ag(I) metallophilic attractions and luminescence of $[Au_2(carb)_2Ag(\mu\text{-}3,5\text{-}Ph_2pz)]$ (with Ph = phenyl, pz = pyrazolate) and $[Au(im)CH_3(pz)Ag_2(\mu\text{-}3,5\text{-}H_2pz)_2]$ (with im = imidazole) complexes

Jesús Muñiz *, Luis Enrique Sansores, Anette Rojano, Ana Martínez, Roberto Salcedo

Instituto de Investigaciones en Materiales, Universidad Nacional Autónoma de México, Apartado Postal 70-360, México, DF 04510, Mexico

ARTICLE INFO

Article history:
Received 3 December 2008
Received in revised form 22 January 2009
Accepted 2 February 2009
Available online 13 February 2009

Keywords:
Metallophilic attraction
Phosphorescence
Spin-orbit effects
MLCT

ABSTRACT

The study of trimeric mixed-metal complexes is of great importance for their potential use in sensor devices and nanoparticle design, due to the fascinating luminescent and catalytic activity properties. The goal of this work is to understand the Au(I)–Ag(I) closed-shell metallophilic attraction and phosphorescent character in the representative Au–Ag complexes $[Au_2(carb)_2Ag(\mu\text{-}3,5\text{-}Ph_2pz)]$ (**1**) and $[Au(im)CH_3(pz)Ag_2(\mu\text{-}3,5\text{-}H_2pz)_2]$ (**2**) through *ab initio* and DFT techniques. The metal–metal intramolecular interactions are ruled by a Au 5d and Ag 4d mixing, while the intermolecular attractions are governed by a Au 6s and Ag 5s mixing, by π-stacking attractions coming from pz groups and dispersion interactions in complex **2**. The phosphorescence reported experimentally may be addressed to MLCT transitions, with intrametallic contributions, where a distortion of the lowest-energy excited state geometry of the monomer and dimer are also involved.

1. Introduction

Mixed-metal clusters have attracted attention due to their unique physical and chemical properties [1,2]. Cyclic trinuclear complexes of transition metal cations are related to metallophilic bonding, host-guest chemistry, supramolecular structures, acid-base chemistry [3–7] and metalloaromaticity [8]. The discovery of trimetallic compounds has brought to light the existence of several luminescent properties such as phosphorescence and related phenomena as solvoluminescence; where systems like the gold trimeric compound $\{[Au\{\mu\text{-}C(OMe)=N(CH_3)\}]_3\}_n$ (**a**) luminescence after the exposure to specific solvents like dichloromethane or chloroform. Compound (**a**) displayed different crystalline oligomeric polymorphs and its structure is an infinite trigonal column with several intermolecular closed-shell Au···Au interactions. Besides, the structure and phosphorescent behavior is unique and it has only been reported in this type of Au(I) carbeniate [9,10]. The $Au_3(MeN{=}COMe)_3$ compound also shows the solvoluminescence property, which behavior has been addressed to intermolecular interactions and the molecular stacks of its corresponding polymorphs [11,12].

Most of these systems present a phenomenon termed *metallophilicity* [13,14], referring to weak attractions among closed-shell cations of mixed-metal centers; with weak intramolecular bonding inside the trimeric ring and also intermolecular interactions. Such interactions are presumably related to the luminescent behavior [13]. Metallophilicity is the generalization of the aurophilic attraction; in which Au cations are weakly bound in complexes with two [15] or more metal centers [16]. The aurophilic and the generalized metallophilic attraction are ruled by relativistic and dispersion effects [14,17,18] and in some complexes, intermolecular forces as hydrogen bonding and π stacking also play a role in the bonding.

The preparation of other complexes of the form $\{[3,5\text{-}(CF_3)_2pz]M\}_3$ with M = Au, Ag and Cu, have also been reported [19]. The trimeric compounds show a remarkable phenomenon known as luminescence thermochromism, consisting of the emission at a certain wavelength at a given temperature, which is red-shifted upon heating of the sample from 4 K to room temperature. This behavior has been associated to a geometry distortion in the excited state as suggested by Vorontsov et al. [20].

The bimetallic Au–Ag clusters have shown to be more effective in catalytic activity than pure transition metal clusters [21,22], this is due to the resistance to poisoning, selectivity and increased activity [23,24]. Interesting optical, electronic and medical treatment properties have also been studied in this kind of bimetallic complexes. Besides, a wide range of gold and silver complexes have also been synthesized, which are promising choices on the design of electronic biosensors and nanodevices. It has been established that this kind of compounds are precursors for the formation of nanogold or nanosilver structures, which are excellent room temperature CO oxidation catalysts. Several molecular Au–Ag compounds containing P and sulfur-donor ligands have been

* Corresponding author. Tel.: +52 55 55 50 1935; fax: +52 55 56 16 07 54.
E-mail addresses: jesus@iim.unam.mx, jesusmuso@yahoo.com.mx (J. Muñiz).

0166-1280/$ - see front matter © 2009 Published by Elsevier B.V.
doi:10.1016/j.theochem.2009.02.002

synthesized. These complexes are coordinated to the metal centers whose ancillary ligands are commonly poisonous to catalysis, resulting in small number of applications.

Complexes $[Au_2(carb)_2Ag(\mu\text{-}3,5\text{-}Ph_2pz)]$ (**1**) and $[Au(TRbz)\text{-}Ag_2(\mu\text{-}3,5\text{-}Ph_2pz)_2]$ (**2**) are representative systems of a series of metal mixed Au–Ag complexes recently synthesized [25]. The series is very soluble in several organic solvents, indicating that they can be used as catalytic agents. The experimental results performed by Mohamed et al. [25] showed that when these complexes are supported on a TiO_2 surface upon reduction and calcination, the formation of nanoclusters is observed.

There are several examples where Au–Ag clusters have been prepared [26–30], as well as Au_nAg_m, Au_nPt_m and $Au_nAg_mPt_r$ clusters with carbonyl ligands [31–33]. For instance, the mixed-metal $[AgAu(mtp)_2]$ (mtp = diphenylmethylenethiophosphinate) [29], and gold–silver polymeric chains like $[\{AgAu(C_6F_5)_2(THT \text{ or benzene})\}_n]$ [27], $[\{Au_3(\mu\text{-bzim-}N^3,C^2)_3\}_2Ag]$ [34] and $[AgAu_2(CH_2PPh_3)_4(ClO_4)_4]$ [28].

The mechanism behind the intramolecular and intermolecular interactions of closed-shell Au(I) and Ag(I) cations in mixed trimeric complexes and the excitations giving rise to their attached luminescence have not been explored. The aim of this work is to contribute to the understanding of the phenomena related to the intramolecular metallophilic attraction and intermolecular stacking observed in trimeric mixed Au–Ag compounds and probable relationships with the phosphorescence seen in experiment.

2. Computational methods

Geometry optimizations were performed with second order Møller–Plesset Perturbation Theory, the MP2 [35] computational method, which explicitly accounts for dispersion effects, important in the description of aurophilic interactions. The Stuttgart small-core pseudorelativistic effective core potential [36] with 19 valence electrons was employed for gold. The ECP was used with the valence triple-ζ plus one polarization type; i.e., the basis set TZVP, which is an optimized contracted Gaussian basis set for Au, calculated [37] with the same methodology than that of the basis computed by Schäfer et al. [38]. Two additional *f*-type polarization functions calculated by Pyykkö et al. [39] were augmented to the basis set ($\alpha_f = 0.2, 1.19$). The first function is a diffuse f orbital necessary for the intermolecular interaction, while the second is a polarization function, important for describing the covalent bonding, involving the Au d^{10} shell. For the Ag atoms, the Stuttgart pseudopotential, with 19 valence electrons was also used, with the basis set calculated [37] with the same methodology than the Schäfer's basis sets [38]. For the rest of the atoms (C, N, O and H), the 6-31++G(2d2f, p) basis set was used [40,41]. This basis sets will be denoted through the paper as B1.

Ground state geometries were also calculated at the Density Functional level in accordance with the following approaches: The *X*α exchange potential given by Slater (denoted in this work as SLDF) [42–44], with the parameter $\alpha = 0.7$, and the functional suggested by Vosko, Wilk and Nusair (VWN), including a correction on local correlation (denoted as SVLDF) [45].

The electrostatic energies were evaluated using the methodology developed by Ziegler et al. [46,47] based on Density Functional Theory. This approach was only implemented with the *X*α functional. The Dirac method [48] was employed to compute the atomic core orbitals, which were maintained unrelaxed in the series of complexes. To reduce the computational cost, the inner core shells were fixed; the shell $[1s^2\text{-}4d^{10}]$ was frozen for Au, $[1s^2\text{-}4p^6]$ for Ag, $[1s^2]$ for C, $[1s^2]$ for N, and $[1s^2]$ for O. The scalar zero-order relativistic approximation (ZORA) was applied in these DFT calculations [49,50], since the relativistic effects play an important role in the systems where metallophilic interactions are present. DFT computations were carried out with the high quality triple-ζ plus one polarization basis set, which is a Slater type basis (STO-TZP). The latter basis sets will be referred through this work as B2.

The excited state calculations were performed using the CIS computational method [51] with the B1 basis set. On the other hand, excited state computations were also carried out with the Time Dependent DFT methodology [52], including scalar relativistic effects at the ZORA level and spin-orbit coupling in the excited state. The latter calculations were performed with the B2 basis set. Orbital populations where calculated in accordance with the NBO method [53].

Those computations performed with the B1 basis set were carried out using the GAUSSIAN03 code [54] and the calculations with the B2 basis set were done with the Amsterdam Density Functional (ADF) package [55,56].

3. Results and discussion

3.1. Structural description

Geometry optimizations were carried out on the trinuclear Au(I)–Ag(I) compounds (**1**) and (**2**) (see Fig. 1). The optimization of the second complex was performed by substituting the phenyl ligands by hydrogen atoms, forming the model $[Au(im)CH_3(pz)Ag_2(\mu\text{-}3,5\text{-}H_2pz)_2]$. It has been shown that this simplification is adequate for complexes containing transition metal atoms [57]. A trimetallic ring with two Au atoms and one Ag atom is formed in compound **1**, while a ring with two silver atoms and one gold atom is formed in compound **2**. Compound $[Au_2(carb)_2Ag(\mu\text{-}3,5\text{-}Ph_2pz)]$ **1** (with carb = carbeniate) was optimized using the perturbative MP2 method and Density Functional Theory with SLDF, SVLDF and B3LYP functionals. The structural parameters are shown in Table 1: The Au–Au bond length is shorter than the sum of the van der Waals radii (3.60 Å), indicating the existence of a weak interaction between the Au(I) cations; i.e., an aurophilic attraction. The Au1–Ag1 and Au2–Ag1 bond distances are 3.24 and 3.28 Å, respectively; which can be interpreted as a metallophilic bonding between the Ag(I) and Au(I) closed-shell cations.

The calculations given at the B3LYP level on the ground state geometry returned a value of 3.347 Å for the Au2–Ag1 bond length, overestimating the value found experimentally (3.242 Å). The Au1–Au2 and Au1–Ag1 bond lengths differ by 19 and 17 pm, respectively. It has been stated that DFT is not an appropriate method to model the aurophilic attraction, since a methodology involving dispersion effects is required, as it is the case with the MP2 method. Nevertheless, recent studies performed by Wang's group [58], show that the aurophilic interaction can be modeled with DFT at the expense of choosing the adequate functional. It was found that the *X*α functional with $\alpha = 0.7$ (SLDF), and the exchange-correlation functional of Vosko Wilk Nusair (SVLDF) reproduce the aurophilic attraction satisfactorily, and the resulting data are comparable with those found at the MP2 level. Taking the latter into account, during the current work, the use of the SLDF and SVLDF functionals was incorporated for the geometry optimization of complexes **1** and **2**. The optimized parameters of the ground state geometry of complex **1** are presented in Table 1 in accordance with the results given by the local functionals. It was found that the SLDF Au–Au and Au–Ag bond lengths differ by about 3 pm from the experimental lengths; while the Au2–Ag1 distance is slightly underestimated by 6 pm. Similar results were found when using the SVLDF functional, which slightly underestimates the metal–metal distance. These results are in agreement with the conclusions made by Wang et al. [58]. The Metal-N bond lengths calculated with

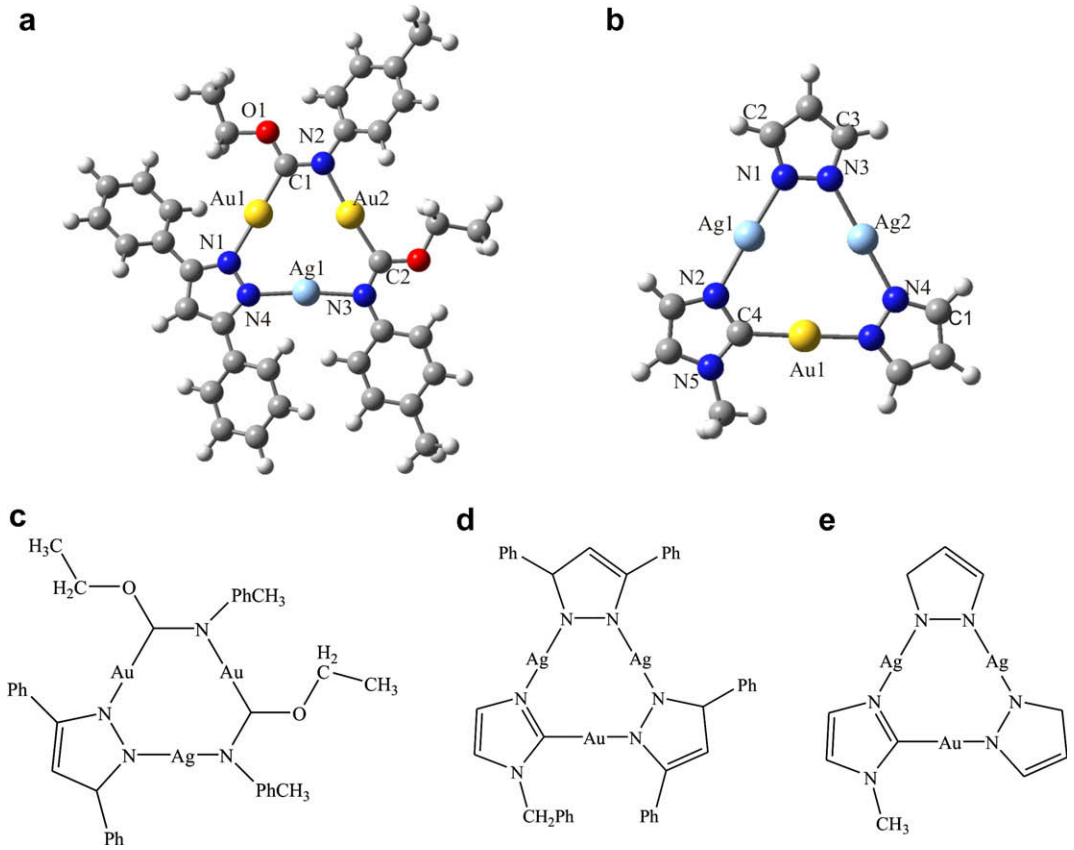

Fig. 1. (a) Ground state geometry of complex **1**, (b) Ground state geometry of complex **2**, (c) Molecular structure of complex $[Au_2(carb)_2Ag(\mu\text{-}3,5\text{-}Ph_2pz)]$ **(1)**, (d) Molecular structure of $[Au(TRbz)\text{-}Ag_2(\mu\text{-}3,5\text{-}Ph_2pz)_2]$ **(2)**, (e) Simplified model of complex **(2)** used for the calculations.

Table 1
Optimized structural parameters of complex **1**.

Bond length	Experimental (Å)	MP2	B3LYP	SLDF	SVLDF
Au1–Au2	3.274	3.453	3.463	3.305	3.225
Au1–Ag1	3.280	3.447	3.455	3.314	3.248
Au2–Ag1	3.242	3.287	3.347	3.178	3.127
Au1–C1	1.980	2.036	2.028	1.980	1.957
Au1–N1	2.064	2.075	2.083	2.031	2.004
Au2–C2	2.006	2.043	2.030	1.985	1.961
Au2–N2	2.035	2.106	2.109	2.068	2.046
Ag1–N3	2.081	2.160	2.143	2.073	2.044
Ag1–N4	2.064	2.140	2.133	2.049	2.020
N1–N4	1.376	1.393	1.385	1.368	1.346
C1–O1	1.344	1.394	1.372	1.360	1.342
N3–C2	1.417	1.326	1.317	1.320	1.302
N2–C3	1.477	1.456	1.447	1.423	1.400
Bond angles (°)					
C1–Au1–N1	177.6	178.5	177.9	178.2	178.0
Ag1–Au2–Au1	60.4	61.4	61.0	61.5	61.5
Au2–Ag1–Au1	60.3	61.6	61.2	61.2	60.8
Au2–Au1–Ag1	59.3	57.0	57.9	57.4	57.8
N4–Ag1–N3	173.77	176.7	178.0	174.5	174.2
Dihedral angles (°)					
C1–Au2–N3–Ag1	12.1	6.1	−1.5	−3.6	−7.4
N2–Au1–N4–Ag1	1.6	1.8	−7.9	−8.2	−9.4

the local functionals are in reasonable agreement with experiment. The differences in the bond lengths computed in this work from those in experiment are due to the fact that the calculations were performed in gas phase, while the experimental values were done in solid state. On the other hand, the calculated bond angles of the ground state are in agreement with those obtained in experiment. As seen from Table 1, the dihedral angles are small, indicating that the molecule presents a structure almost planar in the region of the ring formed by the metallic centers.

The MP2 optimized parameters are similar to those of B3LYP and are poor when compared with the results of the local functionals. The results overestimate the metal–metal intramolecular bond lengths found in the experiment; i.e., in this case the MP2 method appears to be insufficient, as referenced by Pyykkö et al. [59].

The structure of complex **2** was simplified as the molecular model $[Au(im)CH_3(pz)Ag_2(\mu\text{-}3,5\text{-}H_2pz)_2]$ (where im = imidazole and pz = pyrazolate), due to the high computational cost at the MP2 level: The phenyl groups acting as ligands were substituted by hydrogen atoms. The ground state geometry of complex **2** was found at the MP2, SLDF, SVLDF and B3LYP levels (see Table 2). There are no Au–Au interactions in complex **2**. Au1–Ag1 and Ag1–Ag2 bond lengths at the MP2 ground state geometry overestimates by 13 and 18 pm, respectively, the bond lengths found experimentally. The Au1–Ag2 distance differs by only 2 pm. Metal M–N and C–N distances are also in reasonable agreement with those in the crystalline cell.

The bond angles do not undergo significant changes, except for the N2–Ag1–N1 angle, which is 10° larger when computed at the MP2 level. The dihedral angles indicate that at the ground state geometry the complex becomes planar, which is not the case in the crystal cell, where the trimetallic ring is slightly deviated from the plane. This may be due to the absence of phenyl groups, which drives a steric repulsion at the plane of the ring, distorting the planarity; in our calculation, the presence of the hydrogen atoms reduce that effect. In this case, the B3LYP and MP2 results are similar: The M–M bond lengths at the SLDF and SVLDF levels are in agreement with experiment; i.e., the Au1–Ag1 distance differs

Table 2
Optimized structural parameters of complex **2**.

Bond length (Å)	Experimental	MP2	B3LYP	SLDA	SVLDF
Au1–Ag1	3.384	3.515	3.522	3.360	3.290
Au1–Ag2	3.531	3.548	3.566	3.437	3.380
Ag1–Ag2	3.352	3.540	3.520	3.364	3.306
Au1–N5	2.060	2.082	2.077	2.026	2.000
Au1–C1	1.994	2.026	2.015	1.970	1.945
Ag1–N1	2.086	2.135	2.110	2.028	2.003
Ag1–N2	2.100	2.138	2.112	2.030	2.005
Ag2–N3	2.067	2.135	2.107	2.026	2.000
Ag2–N4	2.073	2.134	2.107	2.028	2.002
C1–N4	1.355	1.379	1.363	1.360	1.341
N1–C2	1.345	1.383	1.360	1.357	1.340
N3–C3	1.356	1.383	1.359	1.357	1.340
N5–C4	1.358	1.380	1.358	1.356	1.338
C1–N6	1.359	1.393	1.381	1.374	1.356
Bond angles (°)					
Au1–Ag1–Ag2	63.2	60.4	60.8	61.5	61.7
N2–Ag1–N1	170.3	180.0	179.4	177.4	176.7
N4–Ag2–N3	177.0	178.0	176.7	179.2	179.5
N5–Au1–C1	174.8	179.1	177.3	178.1	178.6
Dihedral angles (°)					
N1–Ag2–N4–Au1	−15.3	1.1	0.3	0.0	0.0
N3–Ag1–N2–Au1	5.1	1.1	0.4	0.0	0.0

only by 1 and 9 pm, respectively, relative to the experimental. The presence of a weak interaction was detected between the Ag(I) cations in the ring, since the bond length is below the sum of the van der Waals radii for silver (3.44 Å) [60]; the Ag1–Ag2 length differs for 1 pm from the experimental value at the SLDA level and it is underestimated by 5 pm at the SVLDF level. The rest of the structural parameters are reproduced satisfactorily.

3.2. Electronic structure

To test the reliability of DFT on the study of metallophilic interactions, we introduced another parameter, which has also been used in the study of aurophilic bonding [61]; that is, the difference between the molecular electron density and the sum of the atomic ground state densities, $\Delta\rho = \rho_{mol} - \sum \rho_{atom}$ at the ZORA level. Contour diagrams of the density difference are depicted in Fig. 2. The contours are plotted on the Au_2Ag and $AuAg_2$ planes of complexes **1** and **2**, respectively. The density distribution describes the chemical nature on the bonding and nonbonding interactions and $\Delta\rho$ is employed to point out that information. An increasing electronic density (see Fig. 2) that ranges from +0.0045 to +0.082 e/Å^3 is seen in the overlapping region among the Au and Ag atoms for complex **1**, while a density increase from +0.0032 to +0.065 e/Å^3 is found for complex **2**. This indicates that an orbital interference coming from the partial filling of the valence 6s-6p and 5s-5p orbitals of Au and Ag atoms, respectively, is taking part in the trimers and inducing weak covalent bonding. This orbital interference was also found for the $[Au_3Cl_3Tr_2]^{2+}$ compound [61].

In solid state, complex **2** show M–M closed-shell intermolecular interactions between the Au(I) and Ag(I) cations. Taking the latter into account, a geometry optimization of the dimer of complex **2** was performed. Considering the high computational cost for this optimization at the MP2 level, this calculation was only performed at the B3LYP and SVLDF levels. The structural parameters are presented in Table 3. It was found that at the SVLDF level, the dimer is certainly bound and the intermolecular metallophilic attraction is reproduced; the intra and intermolecular parameters are slightly overestimated.

The shape of the Hartree–Fock frontier molecular orbitals of the SVLDF ground state geometry of the dimer of complex **2** is depicted in Fig. 3. The HOMO presents a mixture of d_{xz} orbitals of Au and Ag atoms with their respective 6s and 5s orbitals. The MO is located at the center of the trimer ring of monomer **A** (see Fig. 3). The π-orbitals from the pz ligands also contribute in a high extent. The HOMO has also a contribution of the Au 6s and Ag 5s orbital mixture at the region between monomers **A** and **B**. The HOMO–1 presents the d_z^2 orbitals of the metal atoms and a mixture of the 6sp orbitals of the pz ligands on both monomers, but an intermolecular contribution is not present. The HOMO–2 shows a small contribution from the Au d_z^2 and d_{xz} orbitals, while the orbitals from the pz make a π–π interaction allocated on both units of the dimer (see Fig. 3). The intermolecular stacking seen in experiment would be ruled by an intermetallic 6sσ bonding character, which is strengthened by π stacking.

On the other hand, a scanning of the interaction energy as a function of the Au–Ag intermolecular separation was performed, taking into account the basis set superposition error (BSSE) and corrected by the Counterpoise method [62]. The calculation was performed at the MP2 and HF levels for comparison. The results are plotted in Fig. 4: At MP2 level, a minimum located at an intermolecular distance of 3.1 Å was found, which can be addressed to a closed-shell interaction that is consistent with the DFT results. The interaction energy for this molecular geometry is 32.7 kcal/mol; this interaction energy may be interpreted as the 3 contributions coming from the two Au(I)–Ag(I) bonds and the Ag(I)–Ag(I) interaction. Every bonding would have an interaction energy of about 10 kcal/mol; this is an overestimated value, since it is known that the metallophilic energy for Au–Ag and Ag–Ag bonding is of about 6 kcal/mol [39], which represents a weaker value than that of the aurophilic energy (Au–Au bonding), ranging from 5 to 15 kcal/mol [15]. The overestimation may be due to other factors involved in the interaction, such as the energy coming from hydrogen bonding and π-bonding energy.

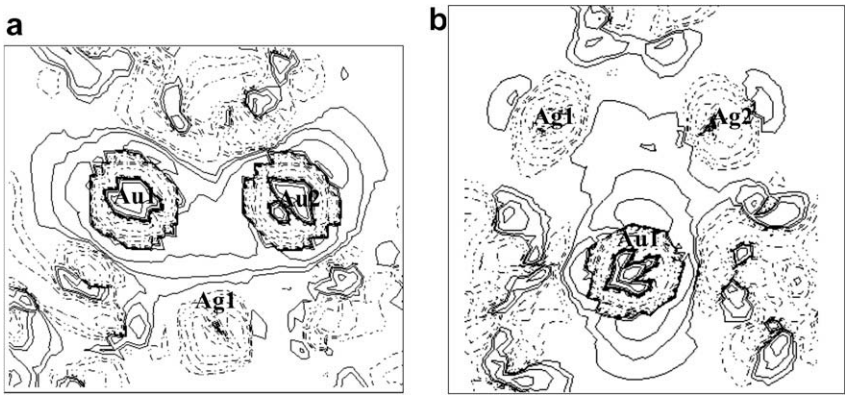

Fig. 2. (a) Contour plot of the difference density ($\Delta\rho$) in compound (**1**) at the plane of the Au_2Ag trimer, (b) Contour plot of the difference density ($\Delta\rho$) in compound (**2**) at the plane of the Ag_2Au trimer. The solid lines refer to regions where the electron density is increased, and the dashed lines refer to regions where the density is decreased.

Table 3
Main optimized structural parameters of the dimer of complex **2**.

Bond distance	Experimental	B3LYP	SVLDF
Intramolecular parameters			
Au1–Ag1	3.531	3.561	3.399
Au1–Ag2	3.384	3.522	3.269
Ag1–Ag2	3.352	3.508	3.268
Au2–Ag3	3.384	3.521	3.269
Au2–Ag4	3.531	3.561	3.399
Ag3–Ag4	3.352	3.509	3.268
Intermolecular parameters			
Ag2–Au2	3.142	4.411	3.000
Au1–Ag3	3.142	4.410	3.000
Ag1–Ag4	3.486	4.580	3.332

The same mapping of the interaction energy was scanned at the HF level, where no minima were found, resulting in a purely repulsive curve and indicating that there are no bound states for the system at this level of theory. This is in agreement with Pyykkö's results [13], stating that the closed-shell interactions are intimately related to the electronic dispersion effects, which are explicitly incorporated in the MP2 formalism.

3.3. Basicity properties

Molecular Electrostatic Potentials (MEP) surfaces have been used to explore the acid/base behavior of trimeric coinage metal complexes with Pyrazolates ligands [19], showing to be a dependable choice to assign acid/base properties. According to the

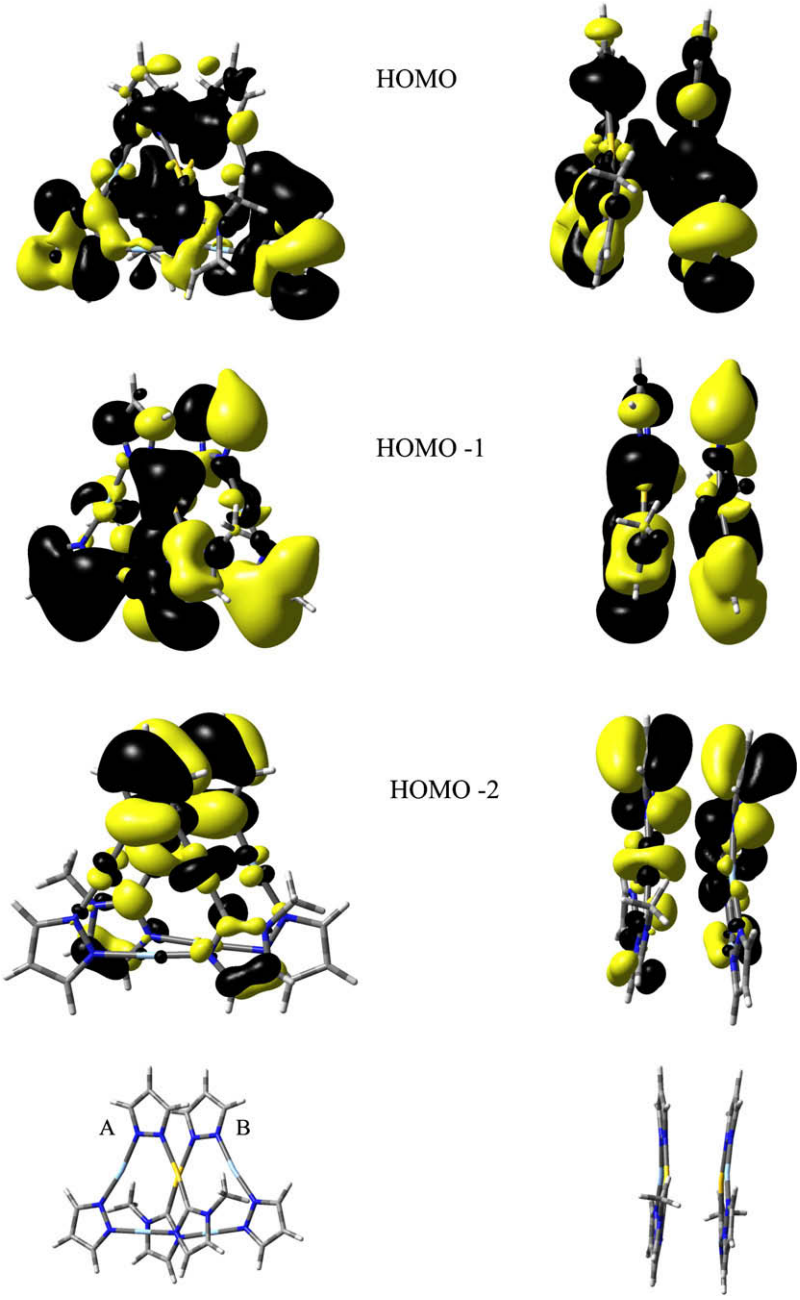

Fig. 3. Frontier molecular orbitals of the SVLDF ground state geometry of complex **2** dimer.

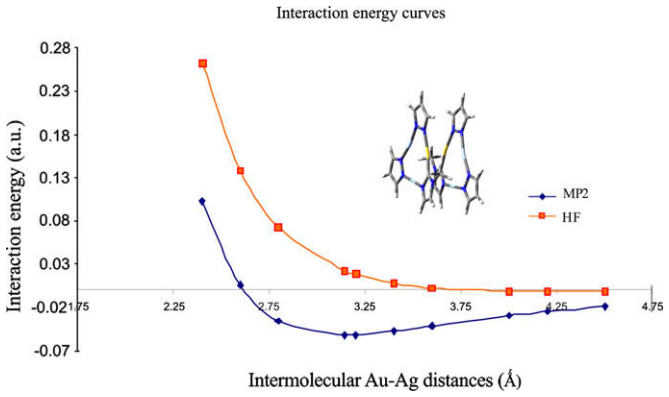

Fig. 4. Interaction energy curves with respect to the intermetallic distance as given by the MP2 and HF levels.

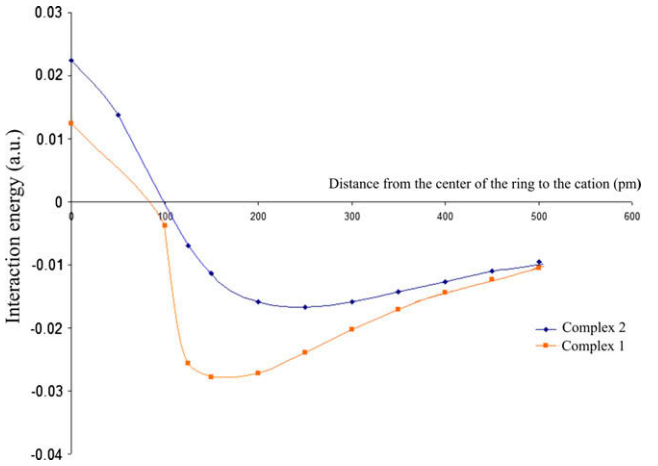

Fig. 6. Electrostatic interaction energy between a positive point charge and complexes **1** and **2**. The point charge moves along an axis perpendicular to the trimer planes.

mapped surfaces presented in Fig. 5, complex **1** has a basic behavior, due to the large negative charge distribution located at the center. On the other hand, complex **2** also presents a basic character, as depicted by the excess of negative electrostatic charge at the center of the ring.

These results are consistent with those found by Omary et al. [19], who assigned a basic behavior to the Au, Ag and Cu trimers with pyrazolate ligands and methane groups attached to them. Complex **2** is only coordinated to a pz ligand; which slightly reduces the basic character of the compound, giving as a consequence a larger density of negative electrostatic charge at the center of the complex. The phenyl groups transfer a certain amount of negative charge to the trimeric ring in complex **1**, strengthening the basic behavior. The latter can be corroborated from the electrostatic energy curves depicted in Fig. 6, computed at the ZORA/SLDF/TZVP level of theory. These curves were computed as a function of the distance from the center of complexes **1** and **2** to a positive point charge. Complex **1** gives a deeper minimum, indicating a greater basic activity. These MEP predictions may be used as a tool to build supramolecular arrangements where the base/acid character of the compounds involved is the dominant mechanism in the bonding. The basic character in the mixed-metal Au–Ag complexes is kept as (**1**) > (**2**), as it is maintained in the pure Au_3 and Ag_3 congeners [19], indicating that the basic behavior in this kind of complexes is essentially ruled by the electronic population on the metal atoms.

3.4. Excited state calculations

According to preliminary experimental studies carried out by Mohamed et al. [25], complexes **1** and **2** are luminescent when exposed to a UV lamp. Complex **1** presents an unreported emission maximum; while complex **2** emits with a maximum centered at 460 nm. The emission is assigned to phosphorescence due to the large Stokes shift, with an absorption band located around 275 nm. To understand the nature of the interaction in the excited state that give rise to the luminescence observed in compound **2**, excited state calculations were carried out using the CIS method with singlets and triplets, starting from the corresponding MP2 and SLDF ground state geometries of the monomer.

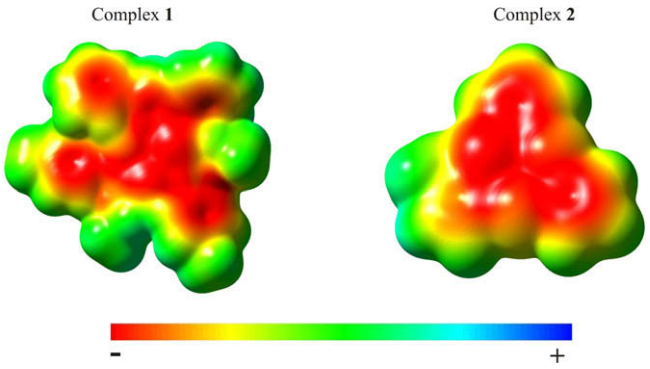

Fig. 5. Molecular electrostatic potential surfaces mapped on the electron density of complexes **1** and **2**.

In Table 4, the first three excitations are presented. The first excited state appeared to be at 197.6 nm (this result is 198.4 nm for the MP2 ground state geometry). This state should correspond to the transition giving rise to the absorption seen experimentally at 275 nm. This interaction corresponds to the transition with the largest oscillator strength (f = 0.36 and 0.39 at the SLDF and MP2 levels of theory, respectively); the oscillator strength (f) is a dimensionless quantity that denotes the intensity of a transition. Considering the excitations from the MP2 geometry, it was found that one of the states with largest CI-coefficient is: (HOMO) → (LUMO + 1).

According to the electronic population analysis, the HOMO is mainly formed by the d_{xz} orbitals located on the Au1 and Ag2 atoms, which represent a 6% and 1% of the total electronic distribution of the MO. In the pyrazolate (pz) ligands, a 93% of the total electronic population is allocated (see Fig. 7). The same analysis can not be applied to the LUMO + 1, since it is a virtual orbital; nevertheless, according to its spatial representation, depicted in Fig. 7, the sites where the electronic charge are transferred in the excited state can be determined. In this case, the charge is transferred towards the 6p orbitals of the metal atoms in the LUMO + 1. Taking the latter into account, the transition can be assigned to a Ligand to Metal Charge Transfer (LMCT) interaction; i.e., the absorption is produced by a charge transfer coming from the pyrazolate ligands and directed to the metal centers. From the electronic population analysis, the slight intrametallic character can not be neglected.

3.5. Optimization of the triplet excited state

From the results experimentally found by Mohamed et al. [25]; the excited state that gives rise to the phosphorescence in complex **2**, comes from a vibronic state, where the molecular geometry is altered in the excited state. To model this kind of interaction, the ground state geometry of the lowest-energy triplet was calculated. This is necessary to understand if the change in geometry at the ex-

Table 4
Excitations at the ground state geometry of the monomer of complex **2**.

Excited state	Multiplicity	Energy (eV)	Wavelength (nm)	*f*
1	Singlet	6.27(6.25)[a]	197.6 (198.4)	0.3589 (0.3890)
2	Singlet	6.55(6.47)	189.4 (191.7)	0.0057 (0.0013)
3	Singlet	6.62(6.51)	187.2 (190.4)	0.0007 (0.0039)

[a] The quantities in parenthesis correspond to the values obtained from the MP2 ground state geometry.

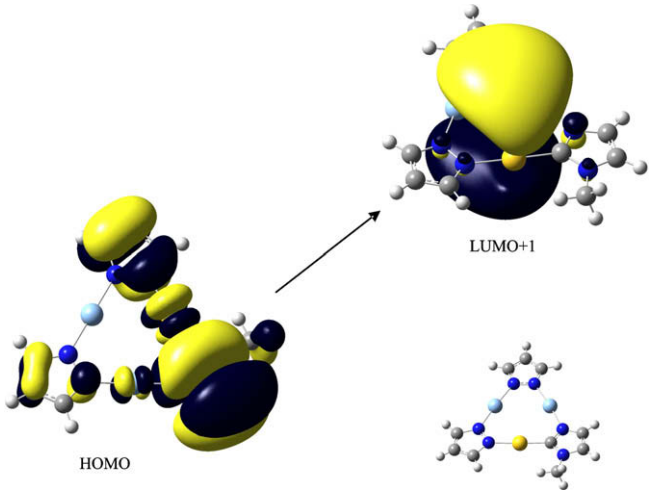

Fig. 7. Single electron transition at the CIS level of the 198.4 nm absorption of complex **2** monomer.

cited state is responsible for the phosphorescence found in experiment. In Table 5, the structural parameters of the optimized triplet are presented.

The optimized geometry of the triplet using both ground state geometries (either MP2 or SLDF levels), is essentially the same. The M–M bond lengths undergo a relaxation from 3.3 to 3.6 Å, and the N5–C4 distance is slightly elongated. The bond angles are kept with no changes, except for the N2–Ag1–N1 angle, which breaks linearity to reach an angle of 176°. The dihedral angles become smaller, giving a flatter geometry on the optimized triplet.

Table 5
Structural parameters for the excited triplet of complex **2**.

Bond length	CIS//MP2	MP2	CIS//SLDF	SLDF
Au1–Ag1	3.636	3.515	3.636	3.360
Au1–Ag2	3.661	3.548	3.660	3.437
Ag1–Ag2	3.640	3.540	3.639	3.364
Au1–N5	2.079	2.082	2.078	2.026
Au1–C1	2.058	2.026	2.058	1.970
Ag1–N1	2.197	2.135	2.197	2.028
Ag1–N2	2.189	2.138	2.189	2.030
Ag2–N3	2.196	2.135	2.196	2.026
Ag2–N4	2.189	2.134	2.189	2.028
C1–N4	1.341	1.379	1.341	1.360
N1–C2	1.336	1.383	1.336	1.357
N3–C3	1.336	1.383	1.336	1.357
N5–C4	1.462	1.380	1.462	1.356
C1–N6	1.363	1.393	1.363	1.374
Bond angles				
Au1–Ag1–Ag2	60.4	60.4	60.4	61.5
N2–Ag1–N1	176.0	180.0	176.0	177.4
N4–Ag2–N3	174.3	178.0	174.3	179.2
N5–Au1–C1	177.0	179.1	177.0	178.1
Dihedral angles				
N1–Ag2–N4–Au1	0.378	1.13	−0.005	−0.027
N3–Ag1–N2–Au1	0.172	1.059	0.013	0.013

A vibrational analysis was performed from the optimized CIS//MP2 and CIS//SVLDF geometries at the triplet state; it was found that all frequencies are real, indicating the existence of true minima. An excited state calculation was then performed from the optimized triplet, the results are presented in Table 6. The first excited state corresponds to a triplet, absent in the excited state calculation performed from the ground state geometry. The excitation is located at 438 nm, and it can be assigned to the emission band observed experimentally (a maximum located at 460 nm). The singlet–triplet excitation is considered a forbidden transition; nevertheless, if the system is excited from a ground state singlet to a singlet excited state ($S_0 \rightarrow S_1$), the system would reach the original ground state again (S_0), and the complex would undergo an inter-system-crossing with a change in the molecular geometry, where the system decays to a triplet state (T_1) of lower energy than that of the excited singlet state (S_1) to finally return to the ground state ($T_1 \rightarrow S_0$).

The LUMO + 1 → HOMO de-excitation represents one of the likely transitions giving rise to phosphorescence. The most probable interaction would correspond to a LUMO + 10 → HOMO de-excitation, which can not be interpreted as a likely transition in nature, due to the large amount of energy released. In consequence, the LUMO + 1 → HOMO transition may be assigned to the phosphorescence seen in experiment. The MOs involved in the interaction are depicted in Fig. 8.

The HOMO on the optimized triplet, is mainly formed by the π orbitals of the pyrazolate ligands and the $d_{xz}\sigma^*$ orbitals located on the metal atoms. The electronic population presents a similar behavior to that of the ground state geometry; this time, a 93% of the electronic population resides on the pyrazolate ligands, and a 6% of the charge is located on the metal atoms. The LUMO is made of the 6p orbitals of the Au and Ag atoms; the charge transfer starts from the metal centers, directed to the pyrazolate ligands; i.e., the phosphorescence can be assigned to a Metal to Ligand Charge Transfer (MLCT) interaction. The series of calculations indicate that the relaxation of the M–M bond lengths give rise to the presence of the luminescence on complex **2**. If the optimized geometry of the triplet is not considered in the excited state calculation, there would be no lower-energy excitation.

3.6. Dimer excitations

The optimized geometry of the dimer of complex **2** was also considered to study the phosphorescent behavior. Using the SVLDF optimized geometry of the dimer, an optimization of the lowest-energy excited state (a triplet) was performed at the CIS level; the main structural parameters are reported in Table 7. It was found that the intrametallic distances in each of the units are slightly elongated, weakening the metallophilic attraction; while the intermetallic distance undergoes a dramatic separation from

Table 6
Excited states of the optimized triplet of complex **2**.

Multiplicity	Energy (eV)	λ (nm)	*f*
Monomer excitations			
Triplet	2.83	438.0	0.0
Triplet	4.34	285.5	0.0
Triplet	4.37	283.5	0.0
Triplet	4.74	261.7	0.0
Triplet	5.28	234.8	0.0
Triplet	5.33	232.6	0.0
Triplet	5.57	222.6	0.0
Triplet	5.87	211.3	0.0
Dimer excitations			
Triplet	2.85	436.0	0.0
Triplet	4.34	286.0	0.0

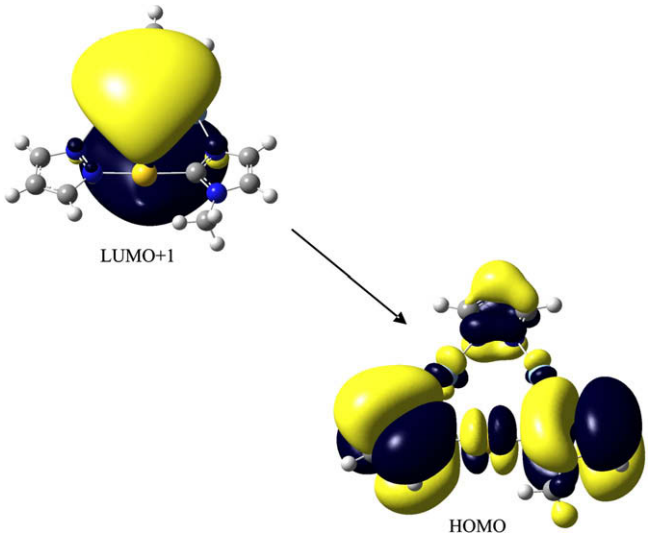

Fig. 8. Single electron transition of the 438 nm phosphorescence of complex **2** (monomer geometry).

an average of 3.111 Å at the ground state, to 4.167 Å at the optimized excited state. In fact, some of the metallic intermolecular interactions are completely absent; i.e. monomer **B** (see Fig. 9) is translated about 1.4 Å from the initial position reported at the ground state and is also rotated to 20° with respect to an axis perpendicular to the plane of the trimer. The intermetallic interactions remaining after geometry optimization at the excited state are Ag2–Au2; Au1–Ag3 and Ag1–Ag4 (see Fig. 9a). Evidently, the bond lengths are longer and the intermolecular metallophilic attraction observed at the ground state is significantly weakened.

From the optimized geometry of the lowest-energy excited state, a CIS excited state calculation was performed; the results are presented in Table 6: It was found that the first excited state shows an excitation energy of 2.85 eV with a wavelength located at 436 nm; whose value can be assigned to the phosphorescence located at 460 nm. The excitations with significant CI-coefficient involved in this interaction are depicted in Fig. 9. The population analysis performed for the occupied MOs indicate that on the HOMO, 54% and 38% of the total electronic charge is located on the π orbitals at the pz and im ligands, respectively, while only a 7% and 1% reside on the d_{σ^*} orbitals of the Au and Ag atoms, respectively. The spatial representation of the virtual MOs gives us a picture of the possible regions around the molecule where electronic charge may reside after an excitation has taken place. It is observed that MOs LUMO + 2, LUMO + 4 and LUMO + 5 have a strong metallic character: LUMO + 2 is mainly composed of the d_{xz} orbitals of Ag and Au atoms with slight contributions from π orbitals located at the pz ligands; while LUMO + 5 is formed by the 6s orbitals of Au and Ag atoms of both monomers; this MO is located at the center of the trimer (see Fig. 8). Finally, MO LUMO + 4 has a stronger 6s character, located at the intermolecular region between the trimeric units.

Table 7
Structural parameters of the optimized lowest-energy excited state of the dimer of complex **2**.

Bond distance	SVLDF[a]	CIS
Intramolecular parameters		
Au1–Ag1	3.399	3.688
Au1–Ag2	3.269	3.630
Ag1–Ag2	3.268	3.660
Au2–Ag3	3.269	3.653
Au2–Ag4	3.399	3.672
Ag3–Ag4	3.268	3.664
Intermolecular parameters		
Ag2–Au2	3.000	4.126
Au1–Ag3	3.000	4.053
Ag1–Ag4	3.332	4.323

Translation of **B** relative to **A**: 1.4 Å.
Rotation of **B** relative to **A**: 20°.
[a] Ground state geometry.

The latter orbital representations indicate that the excitation, giving rise to phosphorescence, can be addressed to a Metal to Ligand Charge Transfer (MLCT), where the intraligand (IL) character has also small contributions. This is consistent with the results found for the monomer of the complex; the calculations obtained for the dimer represent another proof for the vibronic nature of phosphorescence in complex **2**; i.e., the luminescence observed is induced by deformation of the geometry at the optimized triplet. The metallophilic interaction is weakened, extended to intermetallic interactions, which in some cases is completely lost or weakened to a high extent as revealed by the optimization of the dimer in the excited state. We also characterized the emissive process by using the difference in natural atomic orbital populations for the dimer excited state of complex **2** and its respective ground state. It was found that the electronic configuration for the gold atoms 6s(0.85)6p(0.30)5d(9.52) and for the Ag atoms 5s(0.44)5p(0.21)4d(9.74) change in the excited state to 6s(0.77)6p(0.09)5d(9.65) and 5s(0.22)5p(0.09)4d(9.90), respectively. The orbital population of the non-metallic atoms is practically unaltered, which is indicative that the emissive process has an important MMCCT character. In an intra and intermetallic charge transfer, the 6s and 6p occupancy of Au atoms increases by 0.08 and 0.21 electrons, respectively, the Au 5d orbital lose 0.13*e*, which is also transferred to the neighboring Ag atoms inside the single molecule and to the Au and Ag atoms in the other unit of the dimer. An analogous process is present in the Ag atoms of the dimer, where the orbital population of the 5s and 5p orbitals increases by 0.22 and 0.12 electrons and the 4d orbital lose 0.16 in the intermetallic charge transfer.

Mohamed et al. proposed that the phosphorescence observed may be associated to spin-orbit coupling on the heavy-metal centers in the trimeric complex. In order to test this hypothesis, we performed a computation of the singlet to triplet excitations from the optimized triplet of dimer 2 (at the TDDFT level), where spin-orbit effects [55] and the scalar contribution given by ZORA were included. The lowest-energy excitation is a triplet located at 395 nm, which can be associated to the experimental phosphorescence (460 nm). The computed result is quite far from experiment, but it follows exactly the same tendency in the excitations (shown in Table 6); the difference in this calculation is the size of the CI-coefficient, which is much larger than in the CIS computation; in fact, the largest one is 0.9848 for the HOMO → LUMO + 1 excitation, indicating that the interaction is highly probable (the LUMO + 1 also presents a metallic character). An analogous behavior was also predicted at the CIS level with smaller CI-coefficients (see Fig. 9). This indicates that spin-orbit effects may play a role in the lower-energy phosphorescence seen in experiment.

3.7. Excitations of complex 1

Excited state calculations were performed on complex **1** at the CIS level, taking into account the DFT/SLDF ground state geometry, such results are reported in Table 8: It was found that the second excited state presents a high oscillator strength (0.7330), located at 223 nm; such state can be addressed to an absorption band (not reported experimentally). The excitations with the highest CI-coefficients are depicted in Fig. 10. The HOMO is an antibonding orbital with a strong π-character, whose components are mainly located at the N(C_6H_4p-Me) groups and N atoms where a 72%

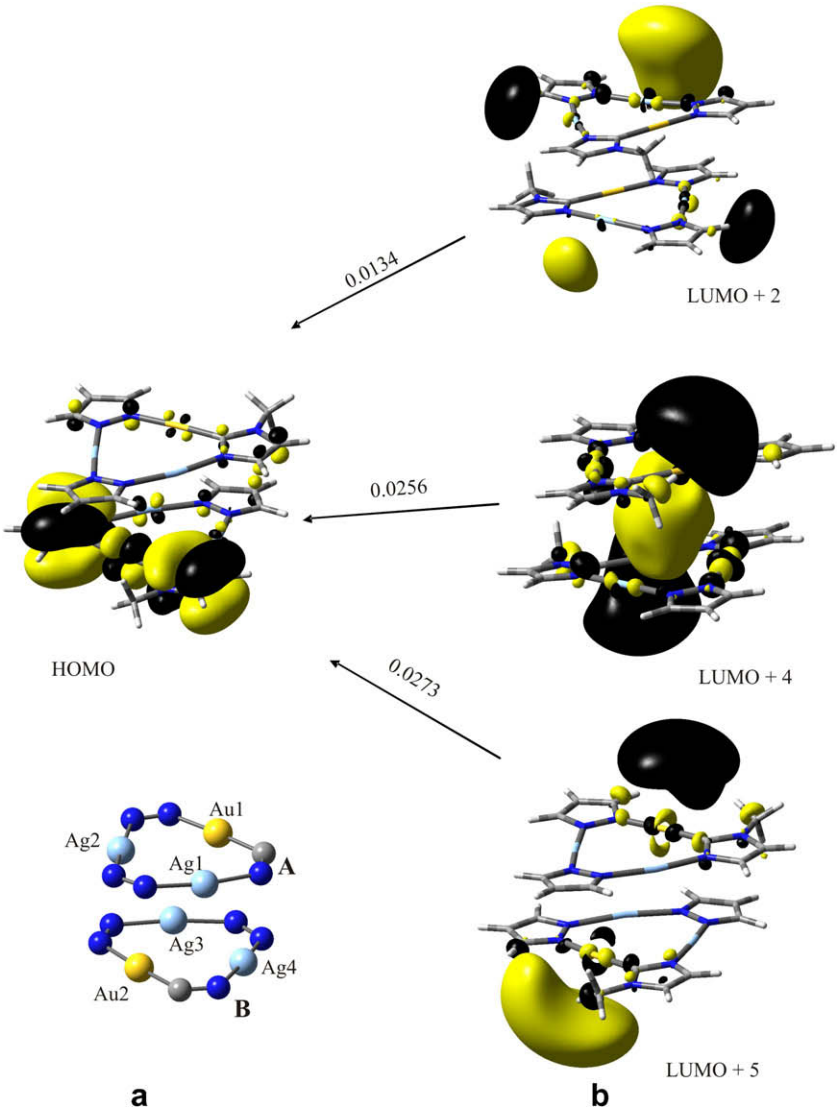

Fig. 9. (a) Molecular representation of the dimer **2** (pz groups have been omitted for clarity); (b) Single electron transition of the 436 nm phosphorescence and the single electron transitions with larger |CI-coefficients| of complex **2** (dimer geometry).

and 12%, respectively, of the total electronic charge is allocated. Besides, the d_{xz} orbitals of the Au atoms and the d_z^2 orbital of the Ag atom participate in this MO with a 1%. On the other hand, in the HOMO–1 also participates the N(C_6H_4p-Me) groups and the π-orbitals from the phenyl groups with 55% and 13% of the total electronic charge residing on them, while the Au and Ag atoms contribute with a 5% and 0.001%, respectively. The shape of the virtual MO indicate that the LUMO is formed by a mixture of Au and Ag 6sp orbitals located at the center of the complex. The LUMO + 1 is composed of interacting d_z^2 orbitals combined with the p orbitals of N atoms and slight contributions from the phenyl π-orbitals. LUMO + 2 (6sp character) presents the main contribution on the Au2 and Ag1 atoms, while the LUMO + 3 shows a combination of the 6s orbitals of Au and Ag atoms located at the center of the ring. Taking the latter into account, the predicted absorption band can be clearly addressed to a Ligand to Metal Charge Transfer (LMCT).

The lowest-energy excited state (see Table 8) is a triplet with an excitation energy of 2.9 eV (416 nm), which can be interpreted as phosphorescence, indicating that compound **1** would be emissive on the blue of the visible spectrum at a low temperature. Considering the energetic levels of the complex, the most likely transitions involved in this interaction are: LUMO → HOMO (0.01366 CI-coefficient); LUMO + 1 → HOMO (0.04304) and LUMO + 2 → -HOMO (0.04366). As it was already stated, the virtual orbitals have a clear metallic character, while the occupied frontier MOs are mainly located on the ligands. Therefore, the excitations giving rise to the predicted phosphorescence would be a Metal to Ligand Charge Transfer (MLCT), where an intrametallic character (Metal to Metal Centered Charge Transfer, MMCCT) is also present as observed from the MO analysis.

Table 8
Excited state calculations of complex **1** at the CIS level.

Energy (eV)	λ (nm)	*f*
Singlet excitations		
5.45	227.3	0.2758
5.56	223.0	0.7330
5.72	217.0	0.0425
5.87	211.1	0.3126
Triplet excitations		
2.98	416.4	0.0
3.05	406.3	0.0
3.15	394.2	0.0
3.91	317.0	0.0

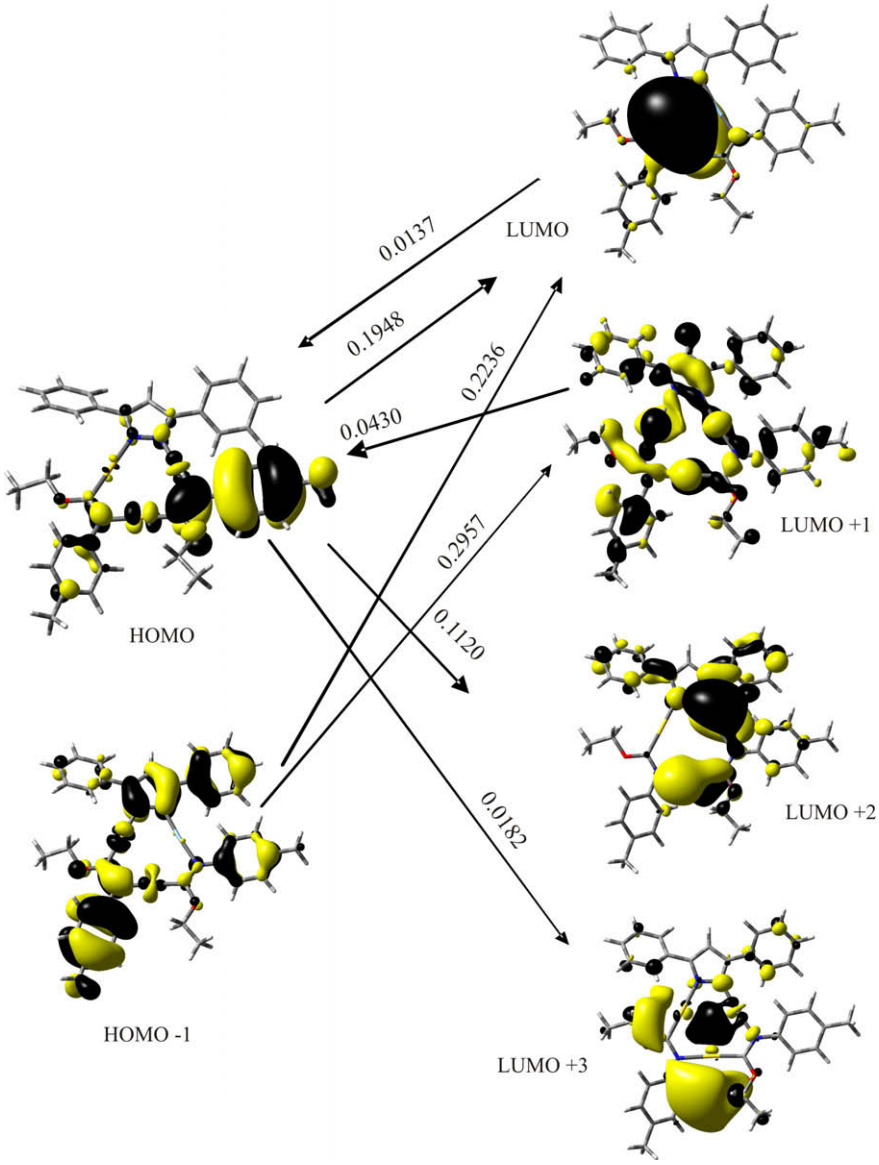

Fig. 10. Spatial representation of the frontier molecular orbitals of the ground state of complex **1**. The single electron transition calculation of the 223 nm absorption and the single electron transitions of the 416 nm phosphorescence with larger |CI-coefficients|.

As it was performed with the dimer of complex **1**, an excited state calculation including explicit scalar relativistic and spin-orbit effects was carried out at the TDDFT level to test at what extent they are involved. It was found, that the lowest excited state is at 3.01 eV (412 nm), which is consistent with the results obtained at the pseudorelativistic level using the CIS method. The computations done at the DFT relativistic level present the following excitations with the highest CI-coefficients: LUMO + 1 → HOMO (0.8324); LUMO + 3 → HOMO (0.0629). The Kohn–Sham orbitals for this interaction have virtually the same shape as the Hartree–Fock orbitals previously found. Therefore, the predicted phosphorescence obtained at this level can also be assigned to a MLCT, in accordance with the results found at the CIS level.

4. Conclusions

A theoretical study on trinuclear Au(I) and Ag(I) complexes was performed: The ground state geometry for both monomers indicate the presence of the Au(I)–Au(I) intramolecular interactions, and the mixed Au(I)–Ag(I) interactions. The closed-shell interactions correspond to an aurophilic attraction and in the general situation (Au–Ag bonding) to a metallophilic attraction. The intramolecular and intermolecular attractions were both modeled at the MP2 and DFT levels of theory, the latter with the careful choice of the functional. B3LYP geometries present slight underestimations on the M–M distances, while the SLDF and SVLDF optimizations give better results. In fact, the local functionals appear to be a more reliable choice than MP2 to model the metallophilic attraction.

Luminescent properties of complex **2** can be explained from the charge transfers taking place in the frontier molecular orbitals in accordance with the CIS excited state calculations. Absorption and emission bands are produced by LMCT and MLCT interactions, respectively. The emission band arises when the excitations are calculated from the optimized excited triplet, i.e., the luminescence is turned on when the geometry is altered in the triplet excited state; and also the spin-orbit coupling plays an important role in the interaction.

Acknowledgements

The authors wish to thank the Impulsa Project, PUNTA; DGSCA-UNAM and Instituto Potosino de Investigación Científica y Tecnológica (IPICYT) for providing computing time. J. Muñiz acknowledges the support from IIM-UNAM under Project No. PAPIIT-IN107807.

References

[1] F. Demartin, C. Femoni, M.C. Iapalucci, G. Longoni, P. Macci, Angew. Chem. Int. Ed. 38 (1999) 531.
[2] R.D. Adams, B.J. Captain, Organomet. Chem. 689 (2004) 4521.
[3] H.V.R. Dias, H.V.K. Diyabalanage, M.G. Eldabaja, O. Elbjeirami, M.A. Rawashdeh-Omary, M.A. Omary, J. Am. Chem. Soc. 127 (2005) 7489.
[4] A. Kishimura, T. Yamashita, T. Aida, J. Am. Chem. Soc. 127 (2005) 179.
[5] M.A. Rawashdeh-Omary, M.A. Omary, J.P. Fackler Jr., R. Galassi, B.R. Pietroni, A. Burini, J. Am. Chem. Soc. 123 (2001) 9689.
[6] J.C. Vickery, M.M. Olmstead, E.Y. Fung, A.L. Balch, Angew.Chem. Int. Ed. Engl. 36 (1997) 1179.
[7] G. Yang, R.G. Raptis, Inorg. Chem. 42 (2003) 261.
[8] L.E. Sansores, R. Salcedo, A. Martínez, N. Mireles, J. Mol. Struct. (Theochem) 763 (2006) 7.
[9] J.C. Vickery, M.M. Olmstead, E.Y. Fung, A.L. Balch, Angew. Chem. Int. Ed. 36 (1997) 1179.
[10] R.L. White-Morris, M.M. Olmstead, S. Attar, A.L. Balch, Inorg. Chem. 44 (2005) 5021.
[11] A.L. Balch, D.J. Doonan, J. Organomet. Chem. 131 (1997) 137.
[12] J.E. Parks, A.L. Balch, J. Organomet. Chem. 71 (1974) 453.
[13] P. Pyykkö, Chem. Rev. 97 (1997) 597.
[14] P. Pyykkö, Angew. Chem. Int. Ed. 43 (2004) 4412.
[15] J. Muñiz, L.E. Sansores, A. Martínez, R. Salcedo, J. Mol. Struct. (Theochem) 820 (2007) 141.
[16] L.E. Sansores, R. Salcedo, H. Flores, A. Martínez, J. Mol. Struct. (Theochem) 530 (2000) 125.
[17] J. Li, P. Pyykkö, Chem. Phys. Lett. 197 (1992) 586.
[18] P. Pyykkö, L. Li, N. Runeberg, Chem. Phys. Lett. 218 (1994) 133.
[19] M.A. Omary, M.A. Rawashdeh-Omary, M.W.A. Gonser, O. Elbjeirami, T. Grimes, T.R. Cundari, H.V.K. Diyabalanage, C.S.P. Gamage, H.V. Rasika Dias, Inorg. Chem. 44 (2005) 8200.
[20] I.I. Vorontsov, A.Y. Kovalevsky, Y.-S. Chen, T. Graber, I.V. Novozhilova, M.A. Omary, P. Coppens, Phys. Rev. Lett. 94 (2005) 193003.
[21] N. Lopez, J.K. Norskov, J. Am. Chem. Soc. 124 (2002) 11262.
[22] B.K. Teo, K.J. Keating, J. Am. Chem. Soc. 106 (1984) 2224.
[23] C.J. Baddeley, M. Tikhov, C. Hardacre, J.R. Lomas, R.M.J. Lambert, J. Phys. Chem. 100 (1996) 2189.
[24] J.L. Rousset, J.C.S. Aires, R. Sekhar, P. Mélinon, B. Prevel, M. Pellarin, J. Phys. Chem. B 104 (2000) 543.
[25] A.A. Mohamed, R. Galassi, F. Papa, A. Burini, J.P. Fackler Jr., Inorg. Chem. 45 (2006) 7770.
[26] R.C.B. Copley, D.M.P. Mingos, J. Chem. Soc. Dalton Trans. (1992) 1755.
[27] R. Usón, A. Laguna, M. Laguna, B.R. Manzano, P.G. Jones, G.M. Sheldrick, J. Chem. Soc. Dalton Trans. (1984) 285.
[28] R. Usón, A. Laguna, M. Laguna, P.G. Jones, C.F. Erdbrügger, Organometallics 6 (1987) 1778.
[29] M.A. Rawashdeh-Omary, M.A. Omary, J.P. Fackler Jr., Inorg. Chim. Acta 334 (2002) 376.
[30] T.G.M.M. Kappen, P.P.J. Schlebos, J.J. Bour, W.P. Bosman, G. Beurskens, J.M.M. Smits, P.T. Beurskens, J. Steggerda, J. Inorg. Chem. 34 (1995) 2121.
[31] N.T. Tran, D.R. Powell, L.F. Dahl, Dalton Tans. 217 (2004).
[32] V.J. Catalano, S.J. Horner, Inorg. Chem. 42 (2003) 8430.
[33] N.T. Tran, D.R. Powell, L.F. Dahl, Dalton Tans. 209 (2004).
[34] A. Burini, R. Bravi, J.P. Fackler Jr., R. Galassi, T.A. Grant, M.A. Omary, M.A. Rawashdeh-Omary, B.R. Pietroni, R. Staples, J. Inorg. Chem. 39 (2000) 3158.
[35] C. Møller, M.S. Plesset, Phys. Rev. 46 (1934) 618.
[36] D. Andrae, U. Haeussermann, M. Dolg, H. Stoll, H. Preuss, Theor. Chim. Acta 77 (1990) 123.
[37] This basis set was calculated by the Stuttgart group and can be accessed via ftp on: ftp://ftp.chemie.uni-karlsruhe.de/pub/basen.
[38] A. Schäfer, C. Huber, R. Ahlrichs, J. Chem. Phys. 100 (1994) 5829.
[39] P. Pyykkö, N. Runeberg, F. Mendizabal, Chem. Eur. J. 3 (1997) 1451.
[40] G.A. Petersson, M.A. Al-Laham, J. Chem. Phys. 94 (1991) 6081.
[41] G.A. Petersson, A. Bennett, T.G. Tensfeldt, M.A. Al-Laham, W.A. Shirley, J. Mantzaris, J. Chem. Phys. 89 (1988) 2193.
[42] J.C. Slater, Phys. Rev. 81 (1951) 385.
[43] R. Gaspar, Acta Phys. Acad. Sci. Hung. 3 (1954) 263.
[44] K. Schwarz, Phys. Rev. B 5 (1972) 2466.
[45] S.H. Vosko, L. Wilk, M. Nusair, Can. J. Phys. 58 (1980) 1200.
[46] T. Ziegler, A. Rauk, Theor. Chim. Acta 46 (1977) 1.
[47] T. Ziegler, A. Rauk, E.J. Baerends, Theor. Chim. Acta 43 (1977) 261.
[48] G. Te Velde, F.M. Bickelhaupt, E.J. Baerends, C.F. Guerra, S.J.A. Van Gisbergen, J.G. Snijders, T. Ziegler, J. Comput. Chem. 22 (2001) 931.
[49] E. van Lenthe, E.J. Baerends, J.G. Snijders, J. Chem. Phys. 101 (1994) 9783.
[50] (a) E. van Lenthe, Int. J. Quantum. Chem. 57 (1996) 281;
(b) E. van Lenthe, A.E. Ehlers, E.J. Baerends, J. Chem. Phys. 110 (1999) 8943.
[51] J.B. Foresman, M. Head-Gordon, J.A. Pople, M.J. Frisch, J. Phys. Chem. 96 (1992) 135.
[52] M.E. Casida, C. Jamorski, K.C. Casida, D.R. Salahub, J. Chem. Phys. 108 (1998) 4439.
[53] E.D. Glendening, A.E. Reed, J.E. Carpenter, F. Weinhold, NBO Version 3.1.
[54] M.J. Frisch, G.W. Trucks, H.B. Schlegel, G.E. Scuseria, M.A. Robb, J.R. Cheeseman, J.A. Montgomery Jr., T. Vreven, K.N. Kudin, J.C. Burant, J.M. Millam, S.S. Iyengar, J. Tomasi, V. Barone, B. Mennucci, M. Cossi, G. Scalmani, N. Rega, G.A. Petersson, H. Nakatsuji, M. Hada, M. Ehara, K. Toyota, R. Fukuda, J. Hasegawa, M. Ishida, T. Nakajima, Y. Honda, O. Kitao, H. Nakai, M. Klene, X. Li, J.E. Knox, H.P. Hratchian, J.B. Cross, V. Bakken, C. Adamo, J. Jaramillo, R. Gomperts, R.E. Stratmann, O. Yazyev, A.J. Austin, R. Cammi, C. Pomelli, J.W. Ochterski, P.Y. Ayala, K. Morokuma, G.A. Voth, P. Salvador, J.J. Dannenberg, V.G. Zakrzewski, S. Dapprich, A.D. Daniels, M.C. Strain, O. Farkas, D.K. Malick, A.D. Rabuck, K. Raghavachari, J.B. Foresman, J.V. Ortiz, Q. Cui, A.G. Baboul, S. Clifford, J. Cioslowski, B.B. Stefanov, G. Liu, A. Liashenko, P. Piskorz, I. Komaromi, R.L. Martin, D.J. Fox, T. Keith, M.A. Al-Laham, C.Y. Peng, A. Nanayakkara, M. Challacombe, P.M. W. Gill, B. Johnson, W. Chen, M.W. Wong, C. Gonzalez, J.A. Pople, Gaussian 03, Revision D.01, Gaussian, Inc., Wallingford CT, 2004.
[55] C. Fonseca-Guerra, J.G. Snijders, G. Te Velde, E.J. Baerends, Theor. Chem. Acc. 99 (1998) 391.
[56] ADF2006.01, SCM, Theoretical Chemistry, Vrije Universiteit, Amsterdam, The Netherlands, http://www.scm.com.
[57] O.D. Häberlen, N. Rösch, J. Phys. Chem. 97 (1993) 4970.
[58] S.G. Wang, W.H.E. Schwarz, J. Am. Chem. Soc. 126 (2004) 1266.
[59] P. Pyykkö, T. Tamm, Organometallics 17 (1998) 4842.
[60] A. Bondi, J. Phys. Chem. 68 (1964) 441.
[61] J. Muñiz, L.E. Sansores, A. Martínez, R. Salcedo, J. Mol. Model. 14 (2008) 417.
[62] S.F. Boys, F. Bernardi, Mol. Phys. 19 (1970) 553.